Full chemical kinetic simulation of biogas early-phase combustion in SI engines

Madan Mohan A.[1*], Anand T.N.C[2], and Ravikrishna R. V[1].

[1] Combustion & Spray Laboratory, Department of Mechanical Engineering
Indian Institute of Science, Bangalore-560012, INDIA.
[2]Department of Mechanical Engineering, IIT Madras, Chennai-600036, INDIA

Abstract

This paper presents computational work on the biogas early-phase combustion in SI engines using detailed chemical kinetics. Specifically, the early-phase combustion is studied to assess the effect of various ignition parameters such as spark plug location, spark energy, and number of spark plugs. An integrated version of the KIVA-3V and CHEMKIN codes was developed and used for the simulations utilizing detailed kinetics involving 325 reactions and 53 species. The results show that location of the spark plug and local flow field play an important role. A central plug configuration which is associated with higher local flow velocities in the vicinity of the spark plug, showed faster initial combustion. Although a dual plug configuration shows the highest rate of fuel consumption, it is comparable to the rate exhibited by the central plug case. The radical species important in the initiation of combustion are identified and their concentrations are monitored during the early phase of combustion. The concentration of these radicals is also observed to correlate very well with the above-mentioned trend. Thus, the role of these radicals in promoting faster combustion has been clearly established. It is also observed that the minimum ignition energy required to initiate a self-sustained flame depends on the flow field condition in the vicinity of the spark plug. Increasing the methane content in the biogas has shown improved combustion.

*Corresponding author: ammohan@mecheng.iisc.ernet.in

1 Introduction

Awareness of limitations of conventional fossil fuel reserves has intensified the search for renewable fuels for use in internal combustion engines. Biogas is one possible alternative for power generation due to flexibility in production from various feedstocks. Since biogas can be produced from agricultural and forest waste, it does not conflict with food production interests[1]. The biogas generated from various feedstocks contains mainly methane and carbon dioxide. Depending on the feed stock and the generation process used, biogas contains 50-80 % methane, 20-50 % carbon dioxide, and trace amounts of Hydrogen and H_2S. The presence of carbon dioxide and other diluents such as N_2 and H_2S with methane reduces the heating value of biogas fuel. The presence of carbon dioxide also leads to reduced effective concentrations of the fuel, CH_4, and of O_2. Carbon dioxide also tends to undergo endothermic reactions that increase rapidly in intensity as combustion temperatures are approached. These endothermic reactions are significant in the early stages of combustion and play a major role on flame propagation. To determine the optimal ignition strategy for biogas-fuelled engines, it is required to understand the in-cylinder aspects of biogas early-phase combustion. Due to the presence of CO_2 which inhibits combustion, ignition delay is expected to be higher, and the burning velocity will be lower. Advancing the ignition timing will resolve the problem of longer delay straightway but may not always be a convenient and viable strategy[2]. Adding fuel additives and increasing the ignition source energy are two other possible methods of accelerating the endothermic phase in the initial phase of combustion[2]. Although, the major part of fuel combustion and heat release take place under highly turbulent

conditions, the initial phase of combustion is very critical for ensuring a self sustained flame and for reducing the time between the initiation of spark and onset of robust, self sustained combustion. During this period, a pool of radical and combustion intermediates must be established to feed the main heat release reactions. The progress of the early combustion phase is closely linked to the detailed chemistry as well as local heat and mass transfer conditions, i.e., the local flow field. Thermodynamic and chemical properties of the non-methane component of biogas, which is primarily CO_2, can also strongly affect the early stages of the combustion due to its non-combustibility.

In literature, most of the studies on biogas-fuelled engines are experimental in nature. Karim and Weirzba[3] conducted experiments using a methane and carbon dioxide mixture as fuel for a single-cylinder, spark ignition engine. It was observed that the maximum power output depends on spark timing and the concentration of carbon dioxide. Huang and Crookes[4] found that with biogas fuels containing a significant amount of CO_2, the engine runs with close-to-stoichiometric mixtures and higher compression ratio gives good performance. The effect of spark plug location and number of plugs in natural gas engines was discussed by Mayer et al.[5]. It was found that a multiple spark plug configuration is better than a centrally located spark plug for maximum power, higher thermal efficiency and low HC production at leaner equivalence ratios[5]. Stone et al.[6] found that the presence of carbon dioxide in biogas lowers the burnt gas temperature, which translates into lower NO emissions. Bertoli et al.[7] linked KIVA-3V [8] and CHEMKIN II [9] to simulate diesel engine combustion with 57 species and 290 chemical reactions. To handle stiff differential equations, a special solver library called VODE was used. Each cell was considered as a continuously stirred tank (CST) adiabatic

reactor which is physically and formally independent from the surrounding cells. Similarly, Yoseffi et al.[2] linked KIVA-3V and CHEMKIN II to simulate a natural gas engine, and found that early stages of combustion are more sensitive to the characteristics of the ignition source than to large changes in fuel composition. Fundamental work on biogas chemical kinetics was performed in counter flow diffusion flames to study the effect of flame stretch on chemistry[10]. Thus, it is observed that most studies on biogas-fuelled engines in literature have been experimental in nature, with few computational studies. Also, there is a specific need to study biogas early-phase combustion in engines since ignition strategies are strongly affected by this phase of combustion. Since biogas early-phase combustion involves complex chemical kinetics, simulations need to be performed using full chemistry. Also, it is not sufficient if the chemistry alone is simulated accurately; the flow field in the engine also needs to be simulated accurately. To the best of our knowledge, the current work is the first reported study where the full chemical kinetics has been taken into account to study the biogas early-phase combustion in SI engines, and additionally, realistic in-cylinder flow field conditions have been utilized in the simulations.

The main motivation behind the present work is to explore ignition strategies for effective combustion of biogas in SI engine. Current experimental efforts require a fundamental understanding of ignition and combustion phenomenon of biogas. This would help in exploring ignition strategies such as spark timing, spark energy, spark plug location and dual spark plugs to maximise engine performance. The present study involves study of the early-phase of combustion in a single cylinder 110-cm^3 four-stroke engine using biogas as fuel. One of the objectives is to explore change in spark timing on

combustion characteristics and engine performance with biogas fuel. In order to simulate the initial phases of engine combustion, KIVA-3V, a specialised multi-dimensional engine simulation program that can simulate turbulence, combustion and moving piston boundary, and CHEMKIN-II, a program for solving species concentration from a multi-step chemical kinetic mechanism are used. The next few sections describe the computational methodology, and a discussion of the results followed by a summary of the key findings.

2 Computational Methodology

To simulate detailed chemical kinetics along with fluid dynamics, the CHEMKIN II code is integrated into the KIVA-3V code. In this way, the linked code offers the well known strengths of KIVA-3V for internal combustion engine calculations, while the treatment of detailed chemistry is addressed by CHEMKIN II. The RNG k-ε model is used to simulate the effect of turbulence on convection and diffusion transport. The integration is done such a way that KIVA-3V passes thermodynamic data and species data to CHEMKIN II to obtain a full chemistry solution. Each grid cell is treated as a constant volume adiabatic reactor for the chemistry solution. This is justified because the cell volume does not change in a computational time step of KIVA-3V, and fluid and thermodynamic interactions are frozen across the boundary during the chemistry calculation. During the chemistry solution, the KIVA-3V time step is taken as the integration time in the CHEMKIN II solver to get updated mixture conditions. The energy released in each cell due to the chemical reactions is calculated and added to the specific internal energy of that particular cell. The new gas phase temperature is then updated at the end of time step in CFD solver which is consistent with KIVA-3V

formulation. A similar approach was used by Yossefi et al.[3,11,12] to simulate natural gas combustion in SI engines and by Kong[13] to simulate DME mixture combustion in a HCCI engine. The governing equations for the constant volume adiabatic reactor[14] are shown Appendix I.

A flowchart outlining the computational steps, and the KIVA-CHEMKIN coupling, is shown in Figure 1. Since the biogas contains methane as the main reactive constituent, a detailed chemical kinetic mechanism for CH_4, GRI 3.0[15] , was used to simulate the fuel combustion chemistry. The mechanism consists of 325 reactions and 53 species. In a typical combustion process, initiation happens when a free radical attacks the fuel molecule. The concentration of such free radicals thus plays an important role in combustion initiation and propagation. From the GRI 3.0 mechanism, the following reactions are identified to be important in this initiation process:

$$O+CH_4<=>OH+CH_3 \quad (R1)$$

$$H+CH_4<=>CH_3+H_2 \quad (R2)$$

$$OH+CH_4<=>CH_3+H_2O \quad (R3)$$

$$CH+CH_4<=>H+C_2H_4 \quad (R4)$$

$$CH_2+CH_4<=>2CH_3 \quad (R5)$$

$$HO_2+CH_4<=> CH_3+H_2O_2 \quad (R6)$$

$$HCO+CH_4<=> CH_3+CH_2O \quad (R7)$$

Thus, the concentrations of radicals HCO, CH, HO_2, O, H and CH_2 apart from OH which is an important radical indicating the presence of the flame zone, are tracked during the

simulations. The high temperature quantitative reaction path diagram (QRPD) for methane-air combustion also indicates that OH, H, and O are important radicals that directly attack the methane molecule[14]. The net reaction rates of the other four radicals considered in the present study are much smaller than those of the above-mentioned radicals. However, they were also included in the discussion since the detailed GRI 3.0 mechanism indicated that these radicals are also involved in a direct reaction with the methane molecule.

3 Results and Discussion

The present study was carried out for a 110 cm^3, single-cylinder, SI engine geometry. Figure 2 shows the geometry of the engine used in the simulations which corresponds to the closed-valve part of the engine cycle. The focus of this work is on the early-phase combustion, and hence, computations start from the inlet valve closure (IVC). The time from the initiation of spark to the time where 10% of the total fuel burnt is considered as the initial phase[16]. In this phase, combustion is predominantly governed by chemical kinetics since the turbulent time scales are lower when compared to chemical time scales. The calculated turbulent time scales are of the order of 10^{-4} s, while the chemical time scales are of the order of 10^{-3} s. The turbulent time scale is calculated by taking the ratio of k/ε while the chemical time scale is the time for the fuel to reach 1/e of its initial value[14,17]. Flow at the ignition location is critical in sustaining the combustion and flame development. The flow field from a CFD simulation of the intake stroke of the engine using the AVL-FIRE software and the real engine geometry was taken at intake valve closure and mapped onto the KIVA-3V grid to simulate engine-like flow conditions. A flow field mapping algorithm developed by Sharma et.al[18] is used in

the present study. The mapping algorithm takes the CFD solution from AVL FIRE and the coordinates of the KIVA-3V mesh as input. Then, the algorithm determines the extent of each KIVA cell and identifies the FIRE mesh nodes lying within each KIVA cell region. Each of such FIRE nodes represents a FIRE mesh cell. The values for each thermodynamic and fluid variable are averaged over the corresponding values at all such FIRE nodes and then assigned to the KIVA node under consideration. A homogeneous mixture composition was assumed at the intake valve closure and the air-fuel ratio was calculated using experimental flow rates of fuel and air. A constant wall temperature of 450 K was used for cylinder head, wall and piston surface. Specifications of this engine are described in Table 1. All computations were performed using a full, 360^{o}, three-dimensional mesh.

As mentioned earlier, simulations were performed with a detailed kinetic mechanism. The important assumption made in the simulations is that the turbulent mixing time scales are small compared to the chemical time scales, implying that the effect of turbulence on the combustion is small. This is a reasonable assumption since the initiation of combustion is known to be chemistry-driven[19]. Various strategies such as variation of spark plug location spark timing, spark energy and dual spark plugs have been studied.

Effect of Spark location

The location of spark plug plays an important role in the flame propagation due to the spatial variation in the local flow field. The local flow field affects the mixing of the hot combustion products and the fresh un-burnt mixture. To study the effect of spark location, various strategies incorporating side, central and dual spark plugs have been

simulated. The spark locations are shown in Fig. 3 along with the velocity magnitude in that plane. The variations in the flow field in a perpendicular plane can also be observed in Fig. 4. The same flow field is used as the initial condition for all the cases simulated. However, there is a difference in the local flow field in the vicinity of each plug which is shown quantitatively in Fig.3. The magnitude of the velocity is higher at the central spark plug location compared to side plug locations. The asymmetry in the flow field is observed due to the swirl and tumble motion inside the cylinder. Computations are performed for an equivalence ratio of 1.1 and spark energy of 150 mJ for each plug. For the dual plug case, the total spark energy is 300 mJ. The results show a higher rate of combustion for the central spark plug location as compared to the side spark plug location. The dual spark plug configuration showed a higher rate of combustion than the other two strategies due to the larger ignition area and energy. The burnt fuel mass fractions for all three cases are shown in Fig. 5. The fraction calculated by taking the ratio of the mass of fuel (CH_4) burnt from spark ignition to that crank angle, to the initial mass of the fuel, is referred to as the instantaneous burnt fraction.

The amount of fuel burnt for the dual spark plug case is almost twice as that for the side spark plug case, but only slightly higher compared to that of the central spark plug configuration. Although spark energy and the area are same for both side and central plugs, the local flow field is markedly different with higher velocities in the case of the central plug, leading to a higher burning rate. This is a very important observation and underscores the importance of the coupling between flow and chemistry even during the initial reaction phase where chemistry and not turbulence plays a major role. The total concentration of some of the radicals, specifically OH, O and H are shown as a function

of crank angle in Fig. 6. It is interesting to note that all the radicals show near-identical trends. The other radicals considered are comparatively much smaller in concentration, and hence their variation is not shown in this figure. Also, it is observed that initially, for the central plug case, the rate of growth of these radicals is slower compared to that for both the side and the dual plug cases. However, the radical concentration for the central plug becomes faster and higher as compared to that for the side plug configuration as time progresses. The initial slow rate for the central plug case is attributed to the local flow field with higher velocities at the spark location which results in a faster dissipation of the spark energy. This makes the ignition progress slower initially, and once a sufficient spark kernel is formed, this strong flow field helps in faster spread of high temperature combustion products and consequent faster combustion. To demonstrate this, the fuel mass fraction contours in the plane of spark are shown in Fig. 7 for various crank angles from the onset of the spark. The flame is observed to propagate more in one direction as compared to the other due to flow field directionality. This is observed for all the three configurations. This effect can be further seen in Fig. 8 (a) and Fig. 8 (b) which show fuel mass fraction and temperature contours, respectively in two perpendicular planes for the central spark plug configuration.

Effect of spark energy

The initial phase of biogas combustion is dominated by endothermic reactions due to the presence of CO_2. This may cause misfire, if sufficient energy is not supplied during the ignition process. The effect of ignition energy is studied for side, central and dual plug configurations for 30° BTDC spark timing. For each case, the effect of three

different ignition energies (100 mJ, 150 mJ and 200 mJ) has been studied. The total spark energy is supplied to the cells, in an area of 1-mm^3 over a six-degree crank angle period from the onset of spark. For the side and dual plug cases, the simulations show that an increase in the ignition energy increases the rate of combustion as evident from the fuel consumption rate shown in Fig. 9 as well as in-cylinder OH radical concentrations shown in Fig. 10. However, for the side plug configuration, the difference in the cases with 150 mJ and 200 mJ is small. Interestingly, for the central plug case with 100 mJ ignition energy, combustion was not sustained. As the ignition energy is increased to 150 mJ, combustion is observed to sustain, and further increase in the ignition energy to 200 mJ results in a faster burning rate and is higher than that for both the side and dual plug configurations with the same ignition energy. This is attributed to variation in the local flow field in the vicinity of the spark. As mentioned earlier, the flow velocity is higher at the central plug location compared to the other spark locations. This high velocity aids in carrying the heat and high temperature products from the spark location. For the lower spark energy corresponding to 100 mJ, the transport of heat and products away from the spark location dominates over local heat release resulting in flame extinction.

Effect of equivalence ratio

In practical situations, the air-fuel ratio of the engine varies widely depending on the requirement. The composition of the fuel and air mixture has a major effect on the combustion velocity and flame development. The variation in composition along with the local flow field alters the initial flame development stage drastically. In the present study, the effect of equivalence ratio on the initial stages of combustion at three spark locations has been studied. Simulations were carried out for equivalence ratios of 0.85 (fuel-lean),

1 (stoichiometric), 1.05 and 1.1 (fuel-rich). All three configurations viz. side, central and dual plugs were considered for each equivalence ratio. In all the cases, the total spark energy supplied was maintained constant at 150 mJ per plug. For the conditions studied, simulation results show that the stiochiometric mixture burns slightly faster as compared to both lean and rich mixtures. This is seen from the amount of fuel mass burnt shown in Figure 11. This trend is in agreement with the experimental findings of Shy et al.[20] for turbulent methane-air flames. At stoichiometric conditions, initially, the central spark plug showed a similar rate of fuel consumption as the dual plug case. However, as time progresses, the dual spark plug configuration shows a higher burning rate than the central plug configuration. The reason for this can be understood by considering the flow field at the time of the spark initiation shown in Fig. 3. It can be observed that the flow field direction at the second spark plug in case of dual spark plug configuration is towards the cylinder head. This makes one of the spark plugs less effective in propagating the hot products and radicals outward. At all the remaining equivalence ratios, the dual plug configuration shows slightly higher burning rates compared to the central plug configuration. This is due to the larger ignition area and presence of two flame fronts. The sum of all the fuel attacking radical concentrations mentioned earlier is shown in Fig. 12. It is interesting to note that the radical concentrations again show the same trend, and are observed to correlate with the overall fuel consumption rate. Overall, the central spark plug performs almost as effectively as the dual spark plug case in consuming fuel in the biogas early-phase combustion across the various conditions studied in the present investigation. This is an important and useful finding especially for small engine

applications where the cylinder head has very limited space to accommodate an additional spark plug.

Effect of biogas composition

The effect of biogas composition is studied using various mixtures of CH4 and CO2. Three different compositions of biogas viz. (i) 65% CH4 + 35 % CO2, (ii) 75% CH4 + 25 % CO2, and (iii) 85% CH4 + 15 % CO2 are considered for the current study. Simulations are performed for the central spark plug case with 150 mJ spark energy. A comparison of burnt fuel fractions for the different fuel compositions at various equivalence ratios are shown in Fig.13 to Fig.15. Simulations showed that increasing the methane percentage in the biogas improves the combustion for all the equivalence ratios studied. Increasing the methane content reduces the inert carbon dioxide in the fuel and hence improves the ignition and combustion characteristics of the fuel.

4 Summary

Detailed three-dimensional simulations of biogas early-phase combustion with full chemistry utilizing 325 reactions and 53 species are reported. Specifically, the study is conducted for a single-cylinder, 110 cm^3, four-stroke engine. Flow field mapping at the inlet valve closure was performed to simulate realistic initial conditions inside the cylinder. The effect of spark plug location, spark energy, dual plugs, and equivalence ratio on biogas early-phase combustion has been studied. The simulations show that the flow field near the spark location has a significant effect on the initial flame and radical growth and consequently, the progress of combustion. The central spark plug configuration showed an improved initial flame propagation compared to the side spark

plug case due to higher flow velocities in the vicinity of the spark location. The dual spark plug configuration expectedly gave the highest rate of fuel consumption, however, the rate exhibited by the central plug is comparable underscoring the importance of spark location. From the detailed mechanism, radicals such as OH, HCO, CH, HO_2, O, H and CH_2 are monitored during the early-phase combustion. The concentration of these radicals is also observed to correlate very well with the above-mentioned trends clearly establishing the role of these radicals in promoting faster combustion. For the central spark plug case, lower ignition energy resulted in flame extinction due to faster transport of combustion products. Thus, it is concluded that the minimum energy required to obtain self-sustained ignition depends strongly on the local flow field conditions. The results also show that biogas early-phase combustion rates are higher for stoichiometric mixtures as compared to both lean and rich mixtures. Increasing the methane content in the biogas has shown improved combustion. The results of the study help in understanding the ignition process in biogas-fuelled engines, and can aid in designing engines with better performance and lower probability of misfire.

Nomenclature:

ATDC: After Top Dead Center

BTDC: Before Top Dead Center

CFD: Computational Fluid Dynamics

CST: Continuously Stirred Reactor

C_v: Constant volume specific heat

$C_{v,i}$: Constant volume specific heat of i^{th} species

DME: Dimethyl Ether

HCCI: Homogeneously Charged Compression Ignition

IVC: Inlet Valve Closure

$k_{f,i}$: Rate coefficient of forward reaction

$k_{r,j}$: Rate coefficient of reverse reaction

m: Mass of the system

N: Number of moles

N_i: Number of moles of i^{th} Species

n: Stoichiometric coefficient

QRPD: Quantitative Reaction Path Diagram

$\dot{Q}$: Rate of heat transfer

SI : Spark Ignition

T: Temperature

t: Time

TDC : Top Dead Center

u: Specific internal energy

$\bar{u}$: Molar specific internal energy

$\bar{u}_i$: Molar specific internal energy of i^{th} species

V: Volume of the system

$\dot{W}$: Rate of work transfer

$\dot{\omega}$: Net production rate of the species

X_i : Species concentration

References

[1] Petrou, E.C.; Pappis, C.P. *Biofuels: A survey on pros and cons, Energy & Fuels*, **2009**, 23,1055-1066

[2] Yossefi, D.; Maskell, S. J.; Ashcroft, S. J.; Belmont, M. R. *A comparison of the relative effects of fuel composition and the ignition energy on the early stages of combustion in a natural gas spark-ignition engine using simulation*, Proc. Instn. Mech. Engrs, part D, **2000**, 214, 383-393.

[3] Karim, G.A.; Wierzba, I. *Methane-Carbon Dioxide mixtures as a fuel*, SAE special publications, **1992**, 921557

[4] Haung, J.; Crooks R.J; *Spark ignition engine performance with simulated biogas-a comparison with gasoline and natural gas*, Journal of institute of energy, **1998**, 71, 197-203.

[5] Mayers, D. P.; King, S. R.; Mayer, R. C.; Liss, W. E. Effects of spark plug number and location in natural gas engines, *ASME Journal of Engineering for Gas Turbines and Power*, **1992**, 114, 475–479.

[6] Stone, G. J.; and Ladommatos N. *Analysis of biogas combustion in spark-ignition engines, by means of experimental data and computer simulation*, Journal of institute of energy, **1993**, 66, 180-187.

[7] Bertoli, C.; DeMarino; P., Belardini, P.; Avolio, G. *A New Parallel Numerically Improved KIVA 3V Program for Diesel Combustion Computations*. International multi-dimensional engine modelling group meeting, March 2003

[8] O'Rourke, P. J.; Butler, T. D.; and Amsden, A.A. *KIVA 3V-II: A computer program for chemically reactive flows with sprays*, LA-11560-MS; Los Alamos National Laboratory, Los Alamos, NM, 1989.

[9] Rupley, F. M.; Miller, J. A.; Kee, R. J. *Chemkin-II: A FORTRAN chemical kinetics package for the analysis of gas-phase chemical kinetics*, SAND89-8009B; Sandia National Laboratory, Livermore, CA ,1991.

[10] Jahangirian, S.; Engeda, A.; Wichman, I.S. Thermal and chemical structure of biogas counter flow diffusion flames, *Energy & Fuels*, **2009**, 23, 5312-5321

[11] Yossefi, D.; Ashcroft, S. J.; Belmont, M. R.; Abraham M.; Thurley R.W.F.; Maskell, S. J. Early stages of combustion in internal combustion engines using linked CFD and chemical kinetics computations and its application to natural gas burning engines , *Combustion Science and Technology*, **1997**, *130*, 171-200

[12] Yossefi, D.; Maskell, S. J.; Ashcroft, S. J.; Belmont, M. R. Ignition source characteristics for natural-gas-burning vehicle engines, *Proc. Instn. Mech. Engrs, part D*, **2000**, *214*, 171-180.

[13] Kong, S.,C. A study of natural gas/DME combustion in HCCI engines using CFD with detailed chemical kinetics, *Fuel*, Vol-86, 2007, 1483-89

[14] Turns, S.R., *An Introduction to Combustion: Concepts and Applications*, 2nd ed., McGraw-Hill: New York, 2000.

[15] Smith, G.P.; David, M.G; Michael, F.; Nigel, W.M.; Boris, E.; Mikhail, G.; Bowman, C.T.; Hanson, R.K.; Song, S.; Gardiner, W.C.Jr.; Lissianski, V.V.; and Zhiwei, Q.; *GRI-Mech 3.0*, http://www.me.berkeley.edu/gri_mech/, Date of access: 08/08/2009.

[16] Heywood, J. B., *Internal Combustion Engine Fundamentals*, 1st ed., McGraw-Hill: New York, 1988.

[17] Law, C. K. Combustion Physics, Cambridge University Press, 2006.

[18] Sharma, C.S.; Anand, T.N.C.; Ravikrishna, R.V.; A methodology for analysis of diesel engine in-cylinder flow and combustion, *Progress in Computational Fluid Dynamics*, **2010** , 10-.3 , 157 – 167.

[19] Ganesan V, Internal combustion Engines, 3rd ed, McGraw-Hill: New York, 2008.

[20] Shy, S.S., Lin, W.J.; Wei, J.C. An experimental correlation of turbulent burning velocities for premixed turbulent methane-air combustion, Proc. R. Soc. Lond. A, 2000, 456, 1997-2019

Appendix I:

The derivation of the governing equations for the constant volume adiabatic reactor is given in this section. Starting with the rate form of conservation of energy equation for a fixed mass system,

$$\dot{Q} - \dot{W} = m\frac{du}{dt} \tag{1}$$

where $\dot{Q}$ is rate of heat transfer to the system, $\dot{W}$ is the rate of work done, m is the mass of the system and u is the specific internal energy. For a constant volume reactor, $\dot{W} = 0$. The equation then becomes:

$$m\frac{du}{dt} = \dot{Q} \tag{2}$$

The system internal energy in terms of system chemical composition can be expressed as

$$u = \frac{U}{m} = \frac{\sum_{i=1}^{N} N_i \bar{u}_i}{m} \tag{3}$$

where N_i and $\bar{u}_i$ are the number of moles and molar specific internal energy of i^{th} species respectively. Differentiation of this equation yields:

$$\frac{du}{dt} = \frac{1}{m}\left[\sum_i \left(\bar{u}_i \frac{dN_i}{dt}\right) + \sum_i \left(N_i \frac{d\bar{u}_i}{dt}\right)\right] \tag{4}$$

Assuming ideal gas behaviour, i.e., $\bar{u}_i = \bar{u}_i(T)$,

$$\frac{d\bar{u}_i}{dt} = \frac{\partial \bar{u}_i}{\partial T}\frac{dT}{dt} = \bar{c}_{v,i}\frac{dT}{dt} \tag{5}$$

where, $\bar{c}_{v,i}$ is the molar constant volume specific heat of species i. The system composition $\overline{N}_i$ can be written as:

$$\overline{N}_i = V\left[\overline{X}_i\right] \tag{6}$$

Therefore,

$$\frac{d\overline{N}_i}{dt} = V\dot{\omega}_i \tag{7}$$

where $\dot{\omega}_i$ is the net production rate of i^{th} species, calculated from the detailed chemical mechanism as follows:

$$\dot{\omega}_i = \sum_{j=1}^{L} \nu_{ij} q_j \quad \text{for } i = 1,2,3,.....N \tag{8}$$

$$\nu_{ij} = \left(\nu_{ij}^{"} - \nu_{ij}^{'}\right) \tag{9}$$

where L is number of equations and $\nu_{ij}^{'}$ and $\nu_{ij}^{''}$ are stoichiometric coefficients on the reactants and products side, respectively, for the i^{th} species and j^{th} reaction. The rate-of-progress variable, q_j, is calculated as:

$$q_j = k_{fi}\prod_{i=1}^{N}\left[X_i\right]^{\nu_{ij}^{'}} - k_{rj}\prod_{i=1}^{N}\left[X_i\right]^{\nu_{ij}^{''}} \tag{10}$$

where k_{fi} and k_{rj} are rate coefficients of forward and reverse reactions, respectively. Substituting Eqns. 5, 6 and 7 into Eqn. 4 after rearrangement, we get:

$$\frac{dT}{dt} = \frac{\left(\dot{Q}/V\right) - \sum_i\left(\bar{u}_i\dot{\omega}_i\right)}{\sum_i\left(\left[X_i\right]\bar{c}_{v,i}\right)} \tag{11}$$

However, for a constant volume adiabatic reactor, $\dot{Q} = 0$. Therefore, Eqn. 11 becomes:

$$\frac{dT}{dt} = -\frac{\sum_i\left(\bar{u}_i\dot{\omega}_i\right)}{\sum_i\left(\left[X_i\right]\bar{c}_{v,i}\right)} \tag{12}$$

This gives the rate of change of temperature in the constant volume adiabatic problem.

Bore	5.3 cm
Stroke length	5.31 cm
Squish length	0.08 cm
Swept volume	110 cc
Compression ratio	9.2

Connecting rod length	9.31 cm
Engine speed	3175 rpm
Inlet valve closure	25° ABDC
Spark Timing	30° BTDC

Table 1- Engine specifications

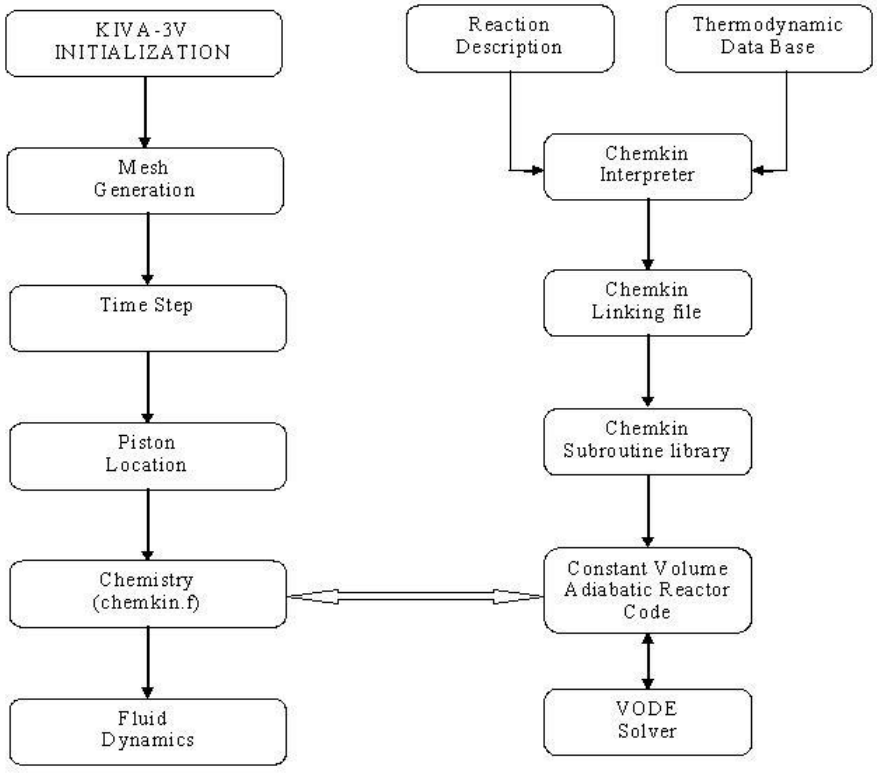

Figure 1: Block diagram of KIVA-3V and CHEMKIN II integration algorithm

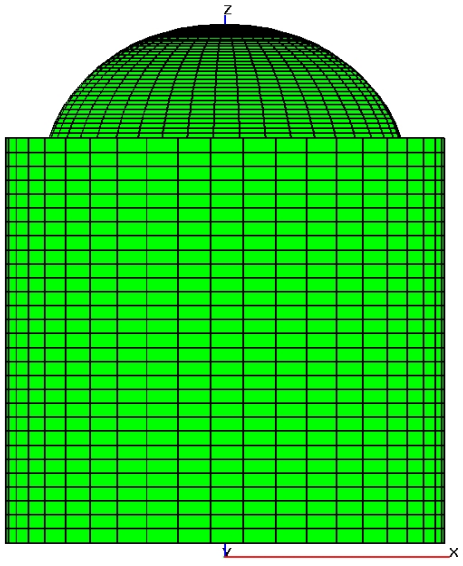

Figure 2: Computational domain corresponding to the in-cylinder geometry at inlet valve closure.

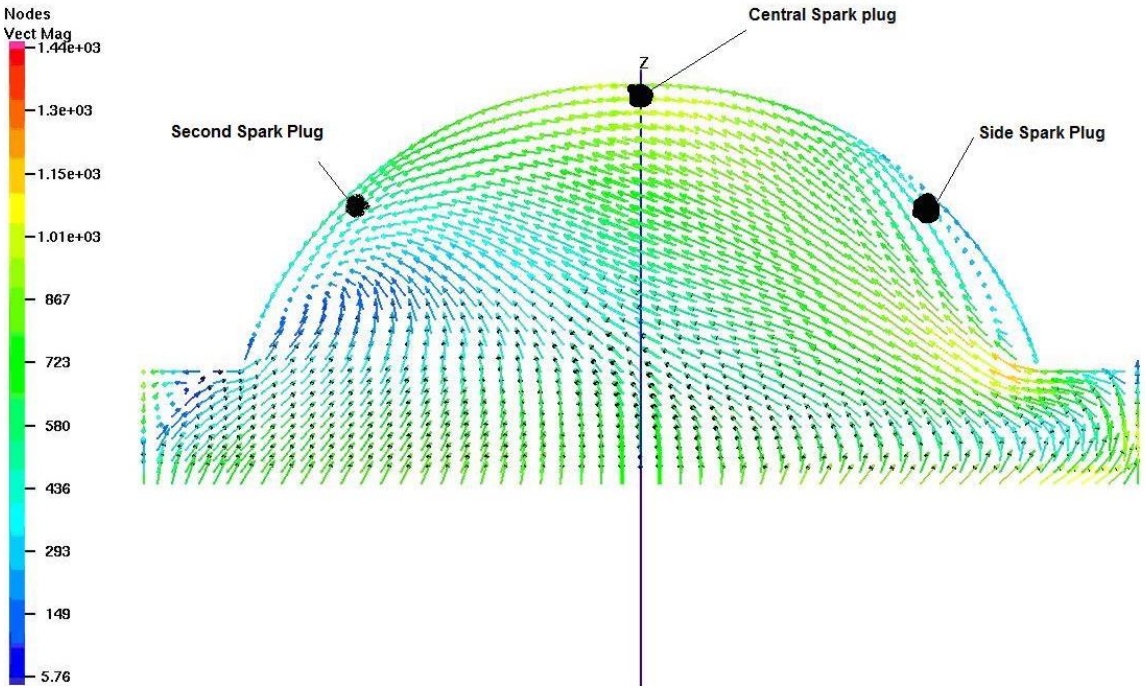

Figure 3: Velocity vectors (cm/s) in a plane passing through the spark plugs at the time of spark initiation.

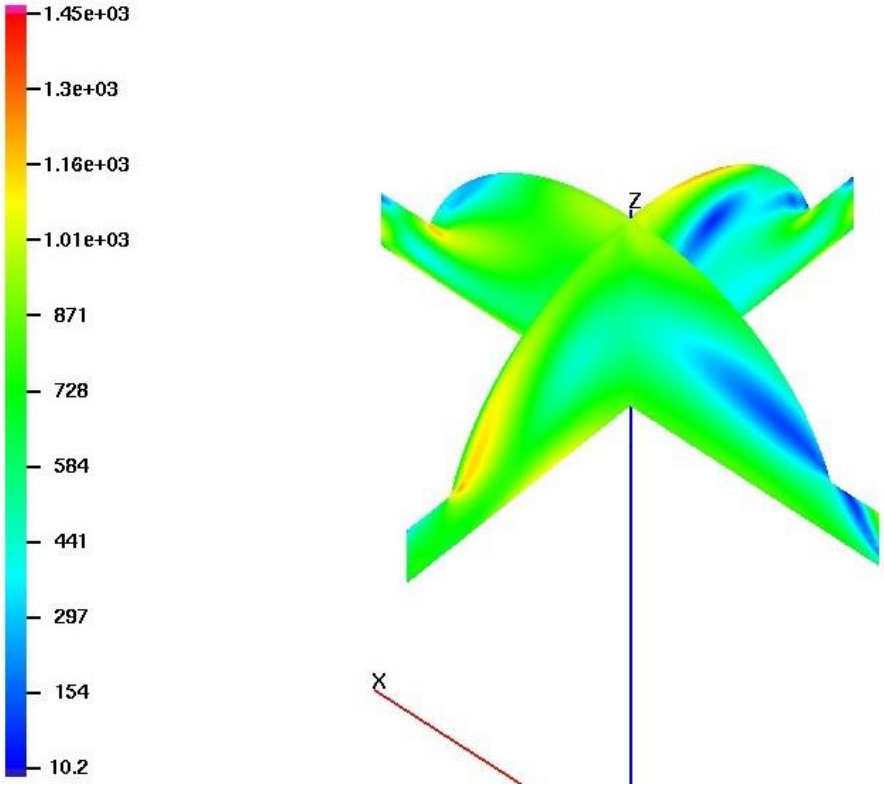

Figure 4: Velocity magnitude (cm/s) in two perpendicular planes at the time of spark initiation

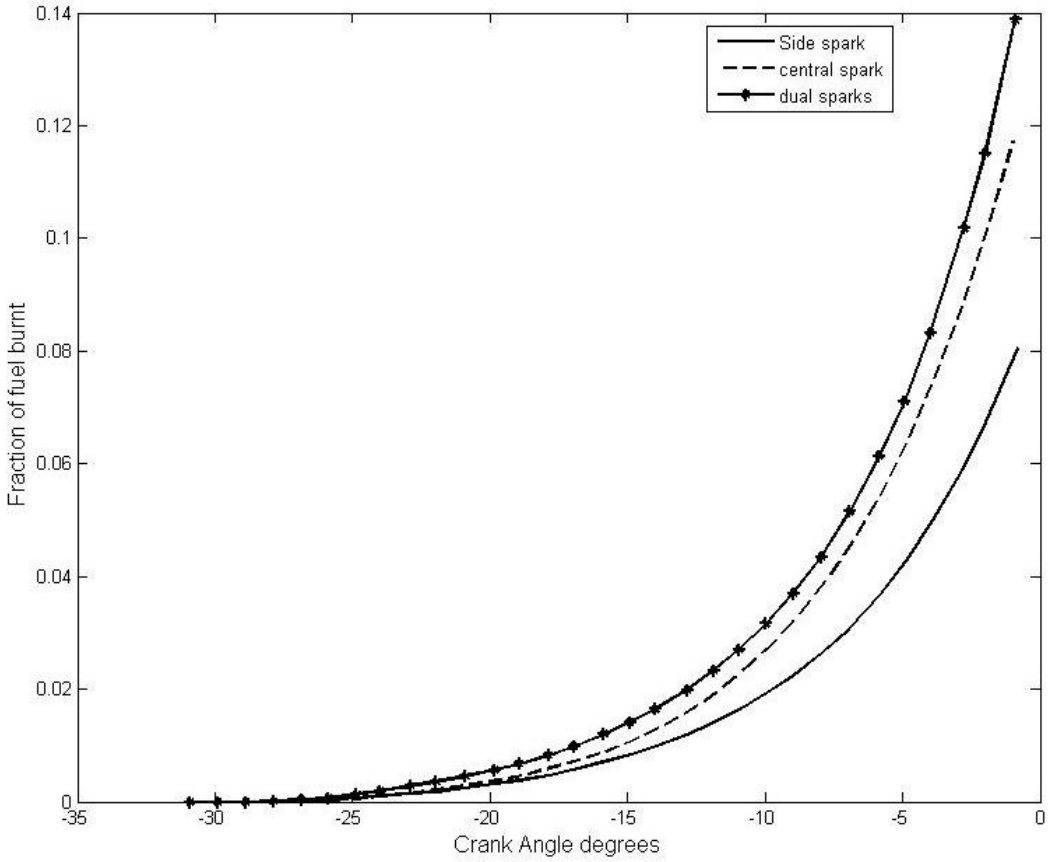

Figure 5: Variation of in-cylinder fuel mass fraction with crank angle

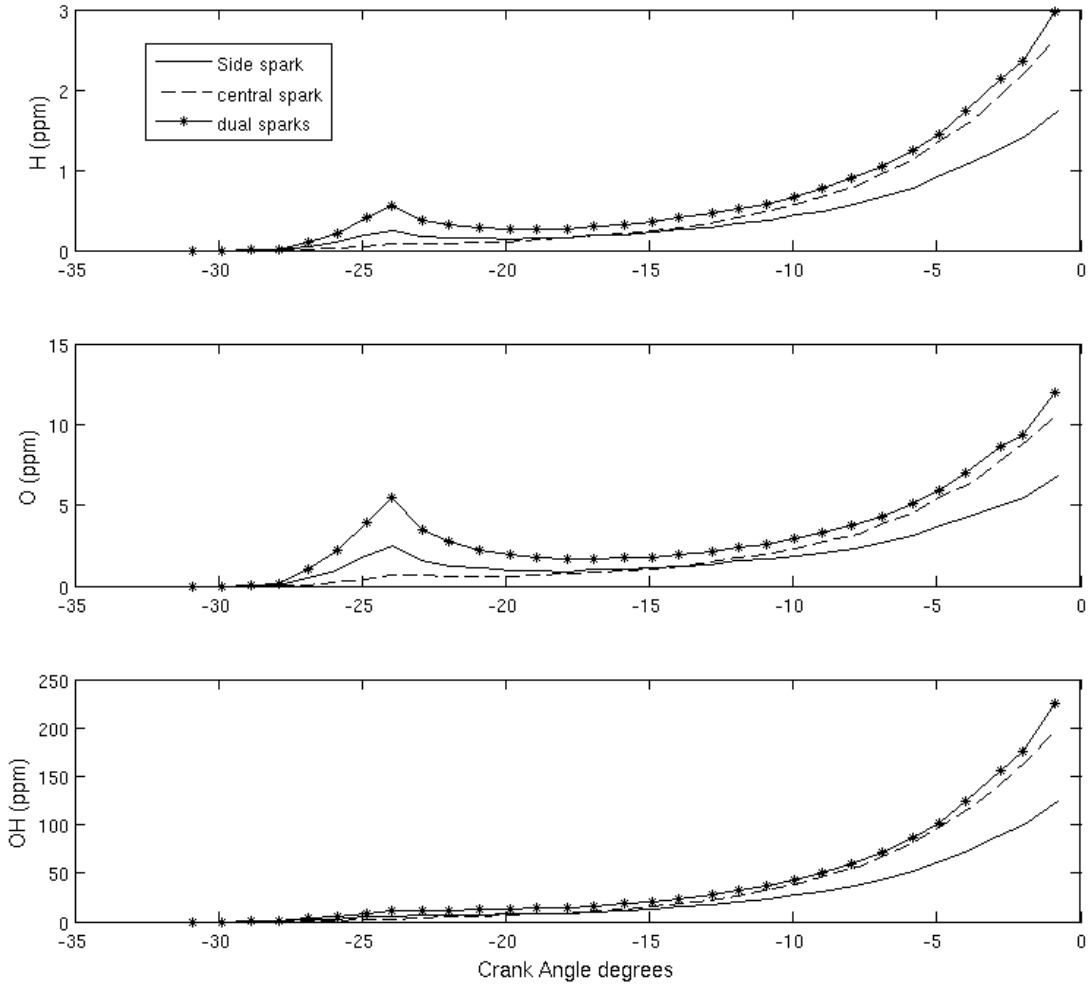

Figure 6: Variation of in-cylinder radical concentration with crank angle

Crank angle from the onset of spark	Side Plug	Central Plug	Dual Plugs	
5°	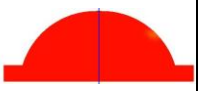	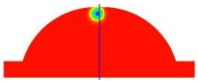	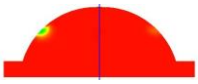	
10°	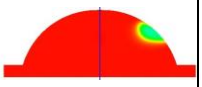	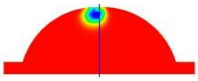	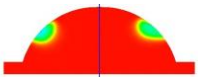	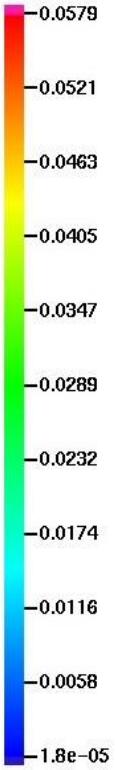
15°	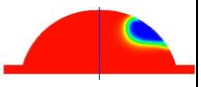	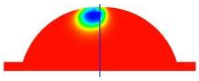	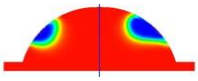	
20°	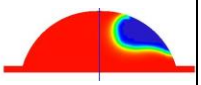	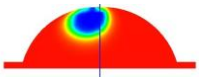	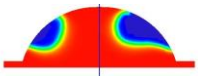	
25°	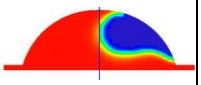	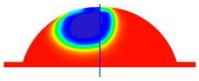	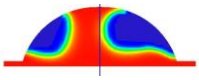	
30°	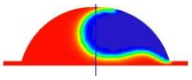	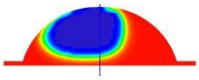	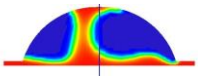	

Figure 7: Fuel mass fraction contours in the plane of the spark location at various crank angles from the onset of spark

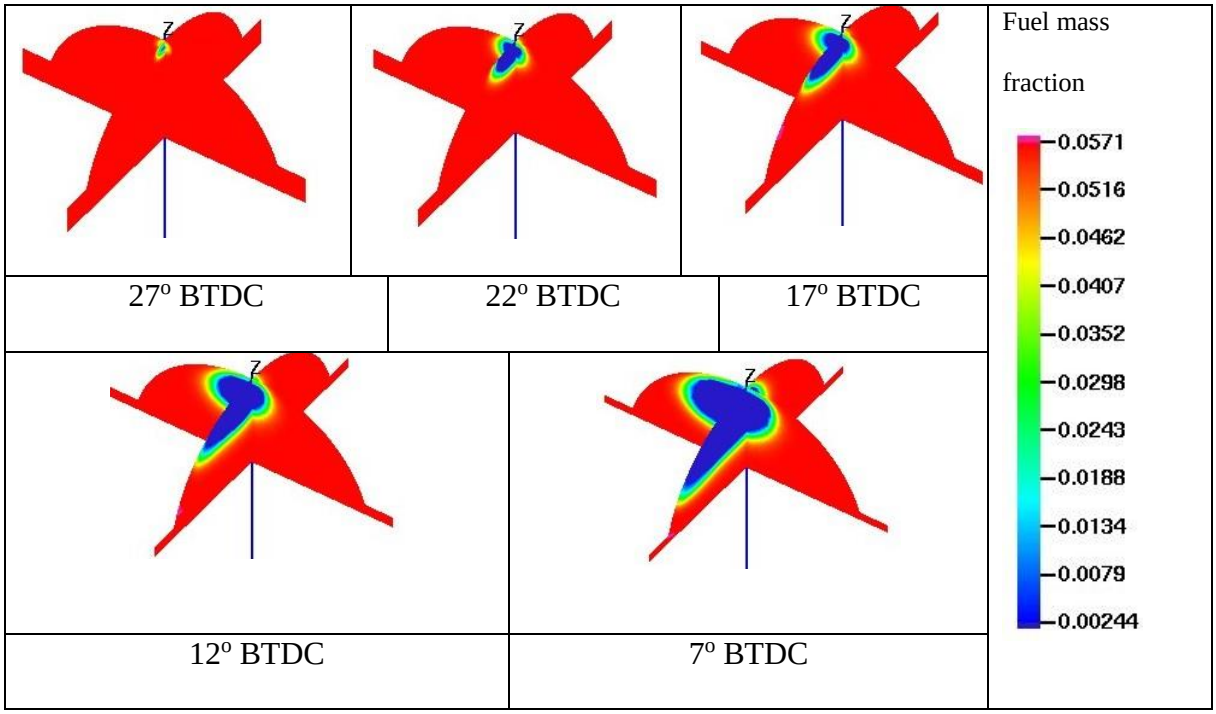

(a)

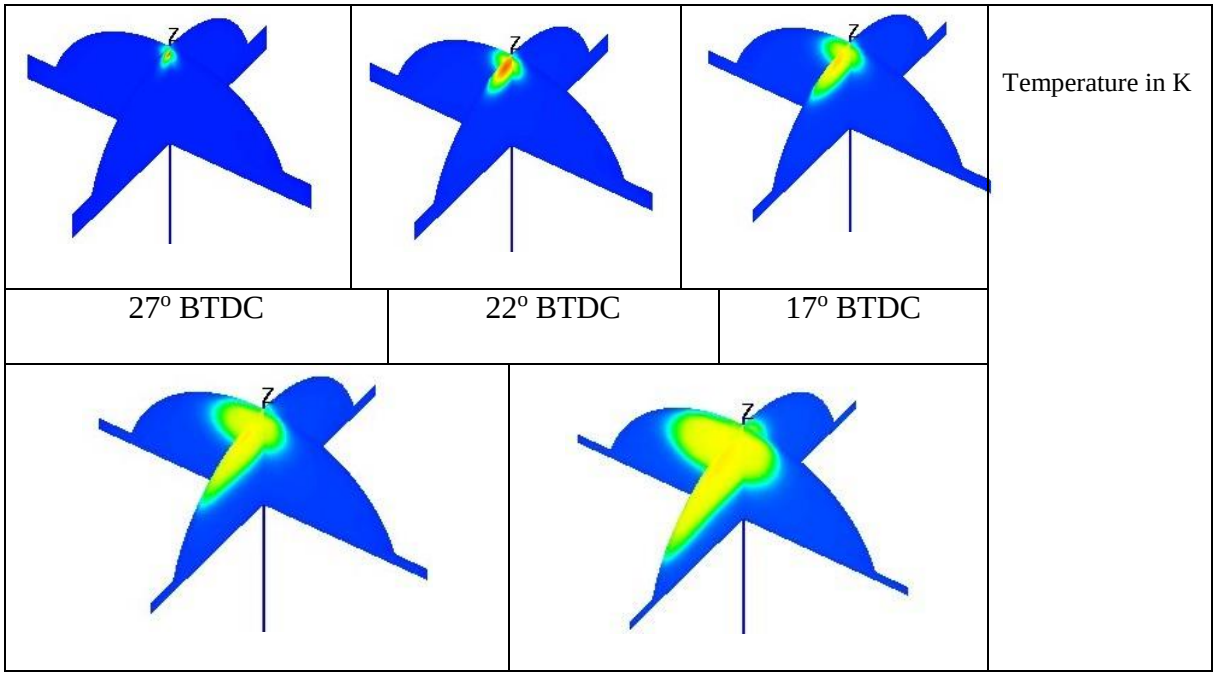

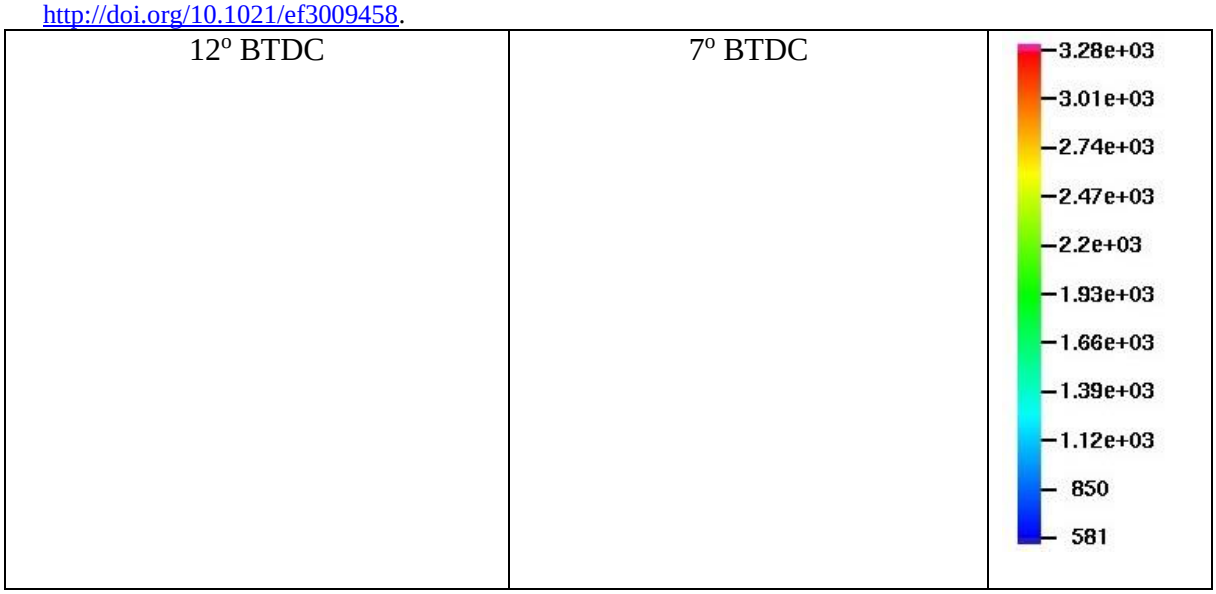

(b)

Figure 8: (a) Fuel mass fraction, (b) Temperature contours in two perpendicular planes at various crank angles for the central spark plug configuration.

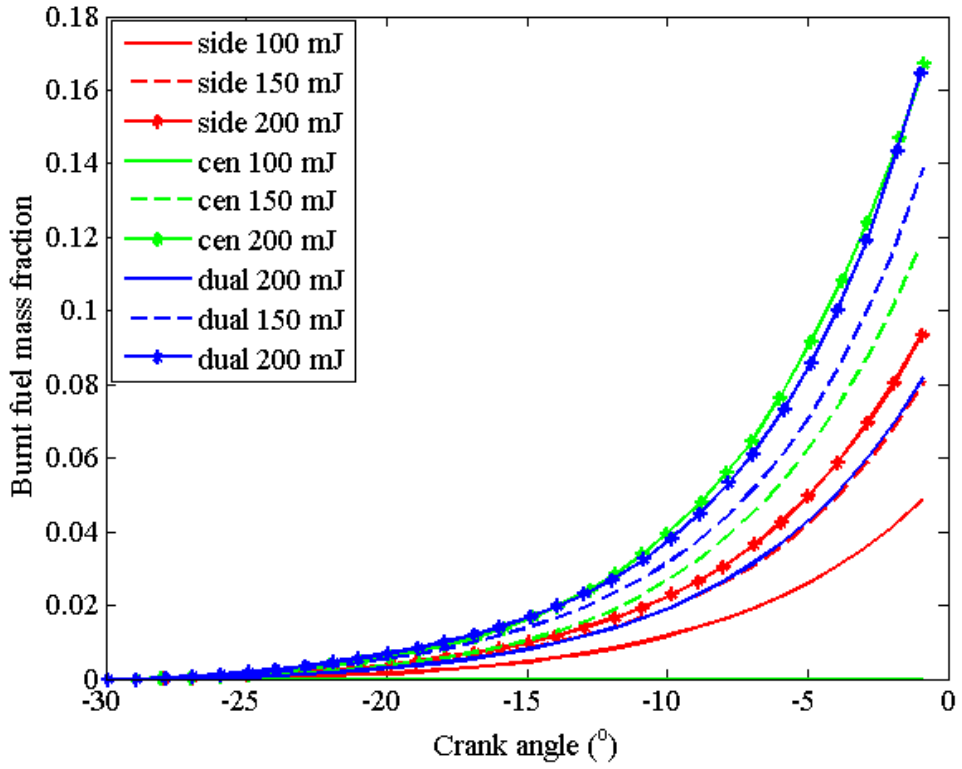

Figure 9: Variation of in-cylinder burnt fuel mass fraction at different spark energies and spark location.

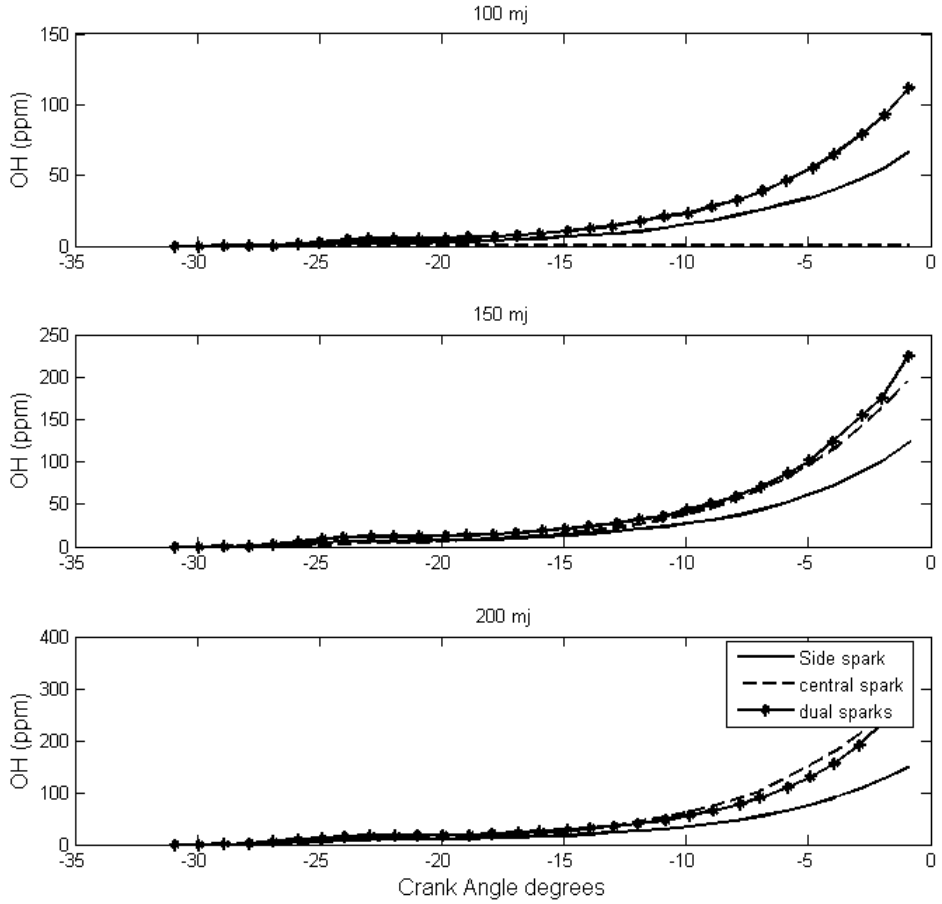

Figure 10: Variation of in-cylinder OH radical concentration corresponding to various levels of spark energy for all three configurations.

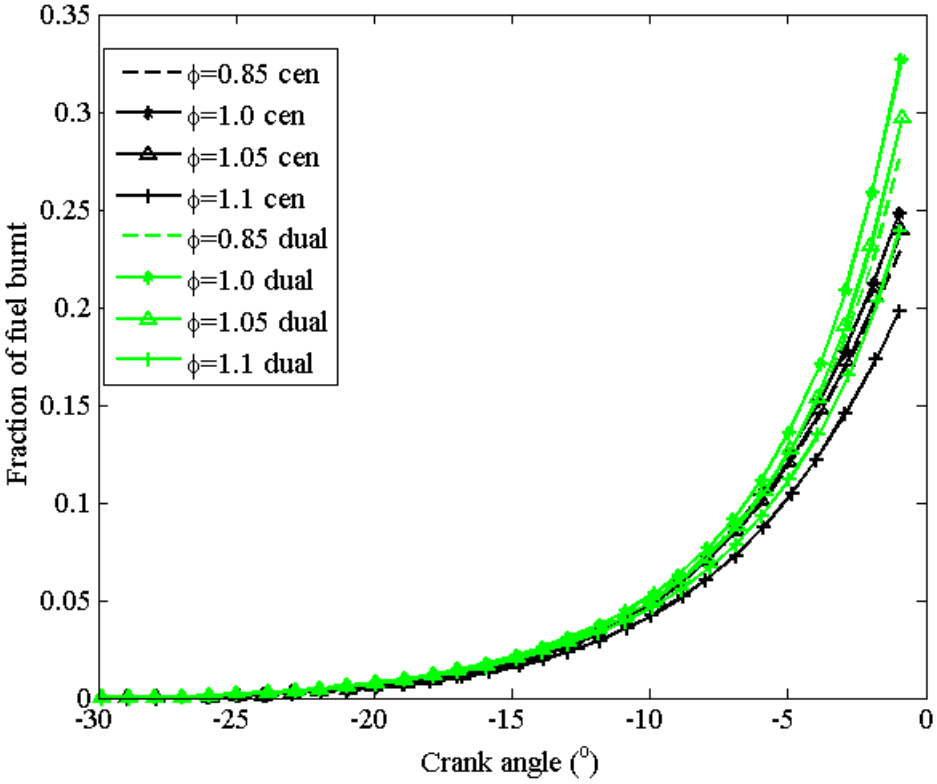

Figure 11: Variation of burnt fuel mass fraction with crank angle for various equivalence ratios.

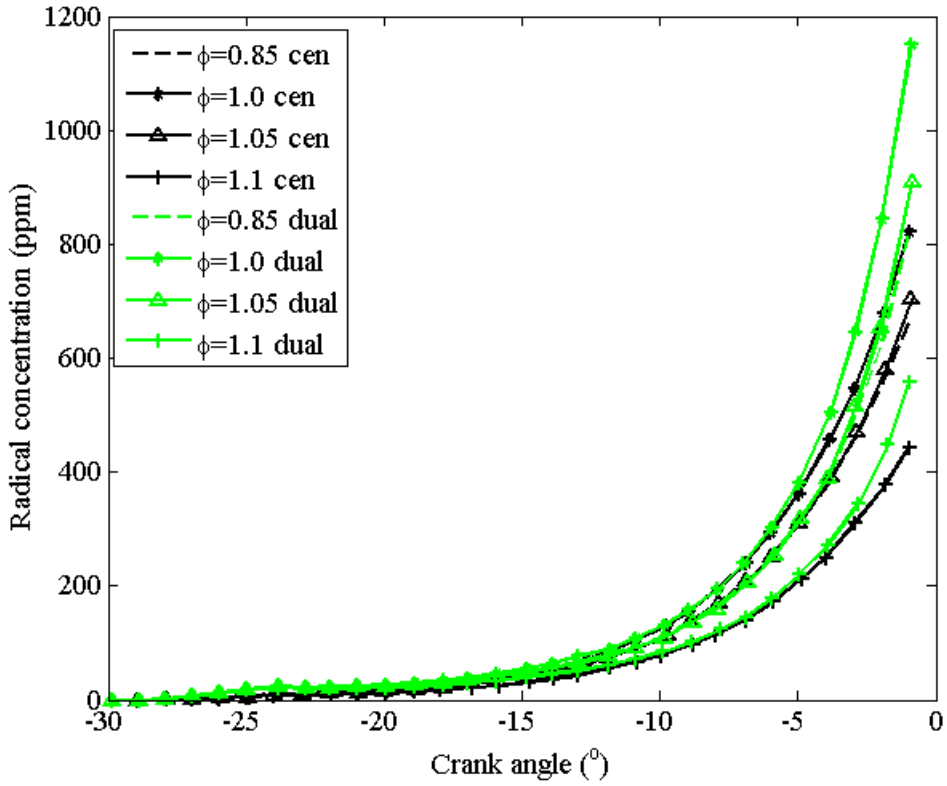

Figure 12: In-cylinder fuel attacking radical concentration for various equivalence ratios.

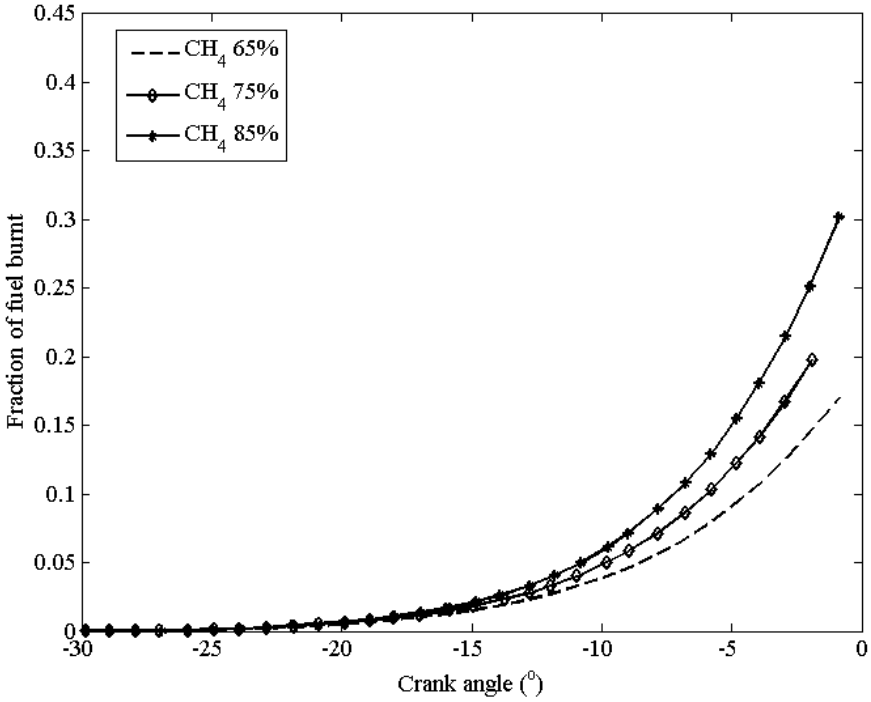

Figure 13: Variation of in-cylinder burnt fuel mass fraction at equivalence ratio0.85

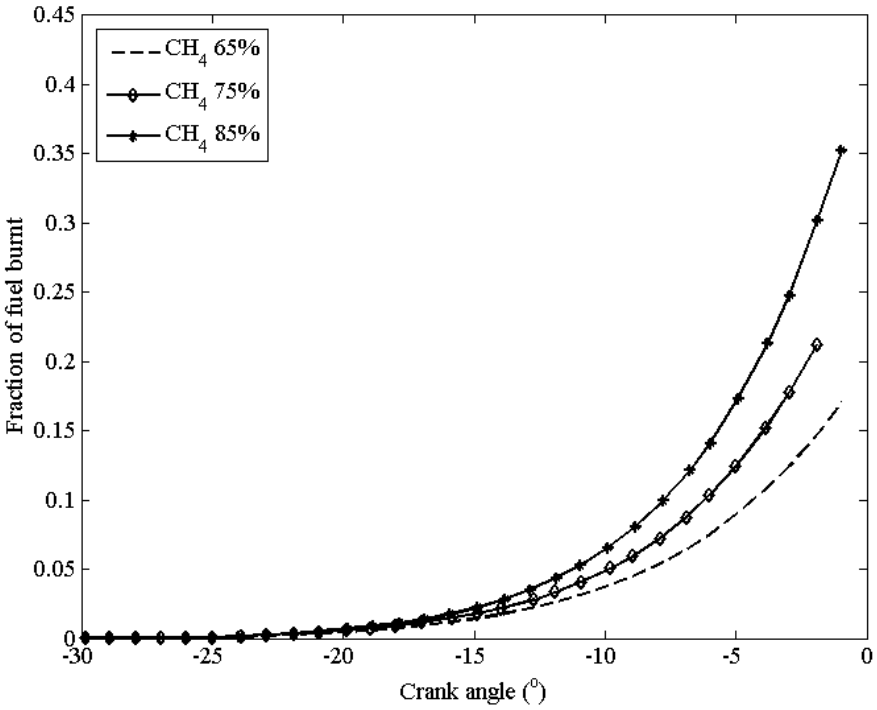

Figure 14: Variation of in-cylinder burnt fuel mass fraction at equivalence ratio 1.0.

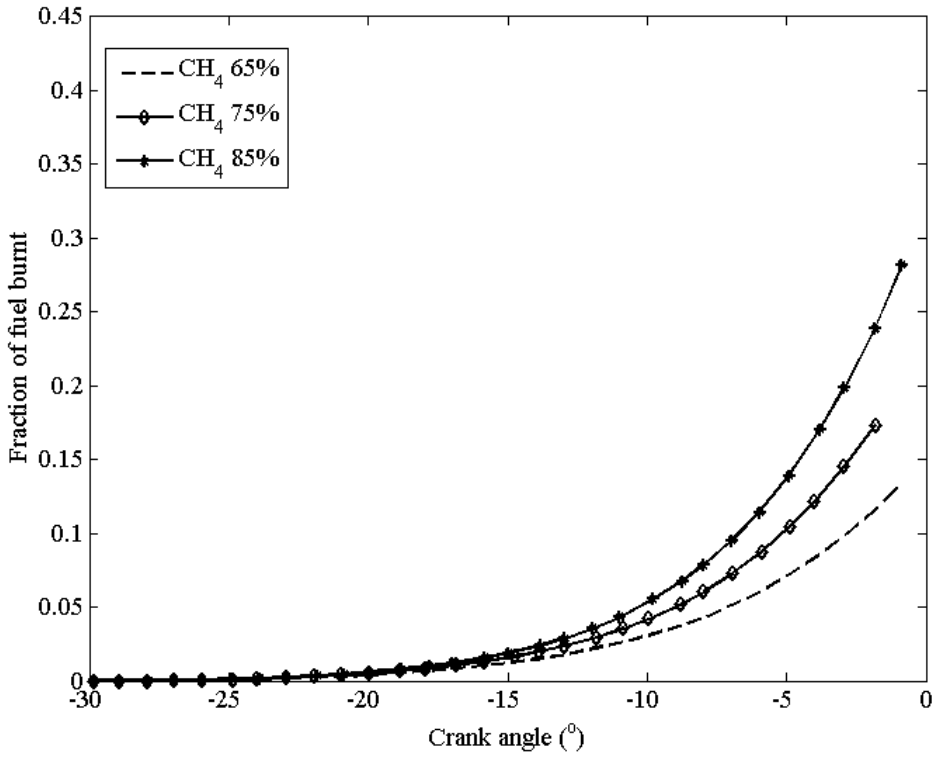

Figure 15: Variation of in-cylinder burnt fuel mass fraction at equivalence ratio 1.1.